
Article:
Amnael Orozco-Díaz, C., Moorehead, R., Reilly, G.C. et al. (2020) Characterization of a composite polylactic acid-hydroxyapatite 3D-printing filament for bone-regeneration. Biomedical Physics & Engineering Express, 6 (2). 025007.

https://doi.org/10.1088/2057-1976/ab73f8

Biomedical Physics & Engineering Express

ENDORSED BY IPEM Institute of Physics and Engineering in Medicine

PAPER • OPEN ACCESS

Characterization of a composite polylactic acid-hydroxyapatite 3D-printing filament for bone-regeneration

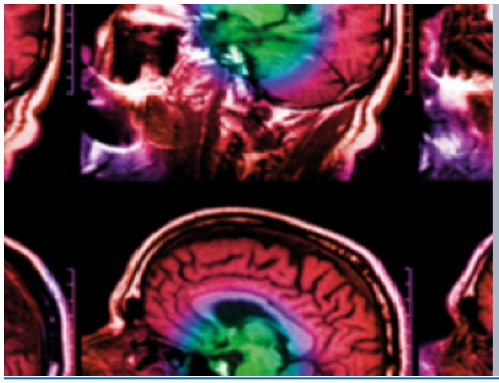

Biomedical Physics & Engineering Express

PAPER

Characterization of a composite polylactic acid-hydroxyapatite 3D-printing filament for bone-regeneration

C Amnael Orozco-Díaz[1], Robert Moorehead[1], Gwendolen C Reilly[2], Fiona Gilchrist[1] and Cheryl Miller[1]

[1] School of Clinical Dentistry, University of Sheffield, Sheffield, United Kingdom
[2] Department of Materials Science and Engineering, University of Sheffield, Sheffield, United Kingdom

E-mail: r.moorehead@sheffield.ac.uk

Keywords: PLA, hydroxyapatite, 3D printing, biocompatibility, mechanical properties, bone regeneration

OPEN ACCESS

RECEIVED
18 September 2019

REVISED
4 February 2020

ACCEPTED FOR PUBLICATION
7 February 2020

PUBLISHED
18 February 2020

Abstract

Autologous cancellous-bone grafts are the current gold standard for therapeutic interventions in which bone-regeneration is desired. The main limitations of these implants are the need for a secondary surgical site, creating a wound on the patient, the limited availability of harvest-safe bone, and the lack of structural integrity of the grafts. Synthetic, resorbable, bone-regeneration materials could pose a viable treatment alternative, that could be implemented through 3D-printing. We present here the development of a polylactic acid-hydroxyapatite (PLA-HAp) composite that can be processed through a commercial-grade 3D-printer. We have shown that this material could be a viable option for the development of therapeutic implants for bone regeneration. Biocompatibility *in vitro* was demonstrated through cell viability studies using the osteoblastic MG63 cell-line, and we have also provided evidence that the presence of HAp in the polymer matrix enhances cell attachment and osteogenicity of the material. We have also provided guidelines for the optimal PLA-HAp ratio for this application, as well as further characterisation of the mechanical and thermal properties of the composite. This study encompasses the base for further research on the possibilities and safety of 3D-printable, polymer-based, resorbable composites for bone regeneration.

1. Introduction

Implants and grafts for surgical reconstruction of the skull vary widely in presentation and characteristics, which are in turn dependant of the clinical requirements of each individual patient, and on how the complex geometries of their cranial bones are affected [1–3]. Some common craniofacial bone defects, such as the alveolar defects on cleft lip and palate (CP) and incidents that warrant orbital floor reconstruction (OFR) pose unique challenges for the production of bone implants to meet their specific therapeutic goals, as well as to suit the irregular geometries and high variability between individual lesions in each case. In both of these kinds of reconstructive surgeries, an implant is required to restore as much mechanical function as possible to the affected bone structures, and restoration of some of the biological functions of the affected site is desirable if at all possible (e.g. self-healing, or tooth eruption).

Given the geometric intricacies that tend to arise from bone defects and lesions, numerous forms of 3D-printing have been gaining interest in research for patient-specific bone-repair devices [4–14]. Defects and fractures are further complicated in skull bones due to their overall thinness, size, closeness to neuro-vascular bundles, and inter-patient anatomic variability. These challenges are currently met with standardised plates, screws, fixtures and other such devises which, though effective, have limitations that must be overcome with careful pre-operatory planning, and in-theatre adjustment of the devices. This results in a natural niche for improvement where patient-specific devices could help improve treatment outcomes or limit complications [15–17]. Evidence for the overall outcome of surgical maxillofacial interventions is more readily available in disease-specific studies, and it has been pointed out that broad areas like facial trauma surgery lack sufficiently evidenced studies in regards of outcomes [17]. Having this in mind, we selected the fore-mentioned applications of CP maxillary reconstruction, and OFR as their expected outcomes, possible complications, and relationship with

implant customisation has been well studied, and they could clearly benefit from the implementation of 3D-printing for bone regeneration.

In CP, most treatment schemes will fit reconstructive surgery of the maxillae within the first 15 years of age of the patient. As such, patients are likely to receive treatment during very active bone growth periods, where maxillary implants have been shown to disrupt normal facial development [18–22], whereas no reconstructive treatment often leads to dental, aesthetic, and psychological issues [20, 23–25]. Currently, the gold standard implant for this surgery is a hip cancellous-bone autograft, which promotes osteogenesis at the implant site [26]. This comes at the expense of the graft-harvest site, where secondary morbidities, including chronic pain, infections and fractures, are common [21, 23, 27–29]. These grafts lack structural integrity and in the long term tend to require a secondary grafting procedure to treat this and other possible complications [22, 29]. On the other hand, autologous grafting bypasses any biocompatibility concerns that are central to the development of materials for long-term implants [30, 31].

OFR techniques regularly use autologous and allogeneic cortical bone implants, but titanium, polypropylene, polyethylene, polytetrafluoroethylene, polyglycolic acid, and PLA are also popular materials for this application [2, 3, 32–34]. In contrast with alveolar repair on CP, the internal floor of the orbit is aims to support the weight of the structures therein—about 43 g [32]. Especially if the lesion compromises the entirety of the orbital floor, meshes and implants used on this context must be able to provide mechanical support for their own mass and the weight of the intra-orbital structures, making cancellous grafts inappropriate for the application and thus limiting options for bone regeneration. Implants for OFR are meant to be permanent, and they have been suggested as contributors in complications immediately following OFR, namely in early-onset retrobulbar haematoma [35].

There has been some growing concern about the implementation of 3D printing on implant production, since official regulations addressing this manufacturing technique are not currently in place [36]. Biocompatibility and biodegradability of polymers such as polylactides—such as the polylactic acid (PLA) used in the present work—have been extensively verified and documented *in vitro* and *in vivo* [30, 31, 37–39]. However, there currently is limited published data on these properties for polylactides processed through fused filament fabrication (FFF) 3D printing. Other molecular-level enhancement techniques such as self-reinforcing have not been noted to affect *in vivo* degradability and tissue response [40, 41]; so it can be hypothesised that appropriate sterilization of machinery and implants is enough to address these concerns. FFF, on the other hand, is not a bulk manufacturing technique, in the sense that the whole mass of the part is processed at once—as in mould casting, for instance. One of the objectives of the present research is to identify the effects the layer-by-layer production process of FFF has on PLA's characteristics as a biomaterial. The FFF workflow we developed has the advantage of not requiring the use of any solvents—as PLA-HA composites regularly do [42–45].

Taking PLA as a structural biocompatible (and mostly bioinert) base for a composite, hydroxyapatite (HAp) was selected as a potential bone-regenerating functionalisation agent. HAp offers micro-scale particulates and thermal-stability at the processing temperatures of PLA 3D-printing filament extrusion and FFF, a consistent affinity for organic molecules, and documented osteoconductive properties [6, 46–50]. The current study will present results from the development for a method for thorough integration of HAp particles into a PLA matrix in the form of a 3D-printable filament. At the time of writing, not many publications have attempted a similar production method for PLA-HAp composites [7, 44, 45, 51]. Some other publications have also dealt with compositing various ceramics into polymer matrixes for a variety of additive manufacturing methods within bone-regeneration [6, 9, 10, 14, 52–55]. Of these, only three publications can be found that have studied with similar composites specifically for FFF with some success [6, 9, 14]. We developed and characterised a bioresorbable 3D-printing filament made of a PLA-HAp composite for the production of bone-regeneration implants, as substitutes for current applications where non-load-bearing autografts are the gold standard.

2. Materials and methods

2.1. Composite filament production

The PLA-HAp composite filament used for this study was produced using a Filabot Original Filament Extruder (Filabot, USA) retrofitted with an external extrusion rate control; an external fan was used for cooling of output filament. This extruder works by taking plastic pellets fed into its top hopper and driving them with a screw into a melting chamber and out from a 3 mm nozzle. The final output was a polymer filament 2.85 to 3 mm in thickness, suitable as feed filament for the BFB-3000 3D printer (3D Systems, USA) implemented in this study.

The composite was produced through weight-to-weight mixtures of High Performance Polylactic Acid 3D Printing Filament (Verbatim, UK) with HAp Captal S hydroxyapatite powder (Plasma Biotal, UK). These raw materials were selected as proof-of-concept proxies for medical-grade materials. The 3D-printing specialised PLA differs from medical-grade lactides in that it is lower molecular weight, which translates to weaker and more flexible mechanical properties: these are beneficial for extrusion and printing. This HAp powder was sintered with a particle size of

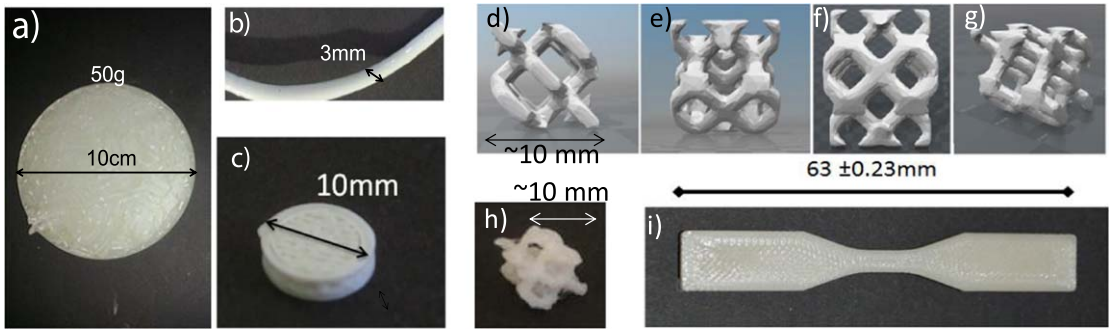

Figure 1. (a) Pre extrusion PLA-HAp solidified mixture as a 5 mm thick disc; (b) 3D-printing filament made of PLA-10%HAp composite; (c) 3D-printed cell culture disc; (d) front view of 3D-model of a 10 mm^3 complex mesh with connected porosity; (e) side view; (f) top view; (g) isometric view; (h) 3D-printed sample of the mesh model made with PLA-10%Hap; i) tensile bar sample specimen.

$D_{50} = 3.59\ \mu$m, selected to be on the lower end of micro-scale HAp after pilot tests with nano-scale powders (data not shown) proved difficult to integrate into the polymer. For production of composite pellets, the raw PLA filament was cut into ∼5 mm segments, manually mixed with the HAp powder in a polytetrafluoroethylene (PTFE) container, and then molten at 185 °C in a drying oven for 3 h. Afterwards, the oven was turned off, and the mixture was then left to cool for at least 6 h to ambient temperature. This resulted in a 10 cm in diameter, ∼5 mm thick composite disc (figure 1(a)) that was then cut down again to ∼5 mm roughly cubic pellets to be fed to the filament extruder (figure 1(b)). This pellet size was selected in accordance to manufacturer's recommendations given the spacing of the extruder's threading.

The HAp to PLA proportions trialled in these experiments were 5%, 10%, and 20% by weight. The extrusion temperature for all of these was set to 190 °C, with the produced filament (∼3 mm in diameter) pulled out and spooled by hand. The extrusion rate and output cooling were manually adjusted during production in order to maintain consistent output diameters and curvatures throughout the filament. Monitoring of these macroscopic characteristics was done by direct inspection as the filament was being extruded. Samples 3D-printed from non-composited, non-treated PLA were used as control throughout the study. For simplicity, these are referred as 'pure PLA' from here on. Figure 1 shows a variety of 3D-printed samples made with the 10%HAp version of the composite, including a complex meshed cube as a test for printability (figures 1(d)–(h)).

2.2. MG63 biocompatibility testing

2.2.1. Cell preparation

MG63 osteosarcoma-like cells were cultured in α-MEM expansion medium (EM) with foetal bovine serum (FBS, 10% volume by volume), 100 IU ml^{-1} of penicillin, 2.5 $\mu g\ ml^{-1}$ of streptomycin, and 2.92 $mg\ ml^{-1}$ of L-glutamine. The cells were incubated in 5% CO_2 at 37 °C in T-72 flasks until >80% confluence was achieved. At that point they were passaged into a new flask, or used for seeding into samples. Cells seeded on samples were cultured in EM for the first 24 h, then switched to a supplemented medium (SM), consisting of EM with added 50 $\mu g\ ml^{-1}$ of ascorbic acid and 10 mM β-glycerophosphate, in order to promote extracellular matrix mineralization.

2.2.2. Cell viability by metabolic activity assay

In vitro testing of the materials was carried out on 3D printed discs of 10 mm in diameter (figure 1(c)); all discs used in these experiments were 3D-printed using a BFB-3000 3D-printer (3D Systems). Discs were seeded with 5000 cells on one of their faces. Seeding was done with the cells suspended on 50 μl of EM, followed by an incubation period of 45 min, and then addition of 2 ml of EM to each sample well. Each iteration consisted of four discs of the material version to be tested. Additionally, control experiments were setup with pure PLA discs as control, and annealed PLA discs were included to investigate if polymer crystallinity had any effect on *in vitro* cell behaviour. PLA discs were annealed in a pre-heated oven at 120 °C for 4 h. Cooling down to environmental temperature was then allowed inside the closed oven.

Samples were then placed in a 12-well cell-culture plate, with one sample per well, laid flat with the face to be seeded facing up. After seeding, they were then covered by 2 ml of OM, completely submerging each disc; plates were left to incubate at 37 °C. Metabolic activity was measured over 21 days using resazurin reduction assays (RRA), and then comparing absorbance readings against a standard curve to determine an approximate cell count. Sampling time periods were set at days 1, 4, 7, 14 and 21 after seeding. This seeding strategy was also used on empty tissue culture plastic (TCP) wells as reference.

For RRA, the samples were stained with 2 ml EM with 27.9 $\mu g\ ml^{-1}$ of resazurin salt (Sigma-Aldrich), and were incubated at 37 °C for 4 h. Excitation-emission measurements were then performed in triplicate

on a Tecan Infinite 200 Pro plate reader at $\lambda_{ex} = 540$ nm and $\lambda_{em} = 590$ nm. Measurements were compared to a RRA-cell number standard curve to estimate cell counts for each sample. This experiment was run twice with triplicate samples (such that $n = 6$). Once the final viability time period was tested, the samples were fixed with a 10% volume by volume formaldehyde solution.

2.2.3. Cell attachment

On day 1 of the viability study, the sample discs were moved to new well plates before RRA staining in order to evaluate only cells attached to the sample. RRA measurements were taken from the original plates, and were compared to a standard curve to estimate the number of cells left on each well after removal of the sample discs, giving an estimate of seeding efficiency.

2.2.4. Calcium and collagen deposition

In order to evaluate *in vitro* osteogenic activity of the MG-63 cell line, measurement of extracellular matrix deposition and mineralisation of said extracellular matrix were measured. To this end, Alizarin Red S assays (ARS, Sigma-Aldrich) were used to evaluate the calcium deposition achieved by the MG63 cells at culture day 21. Samples were fixed in a 37% formaldehyde solution, and then were submerged in a 1% weight-by-volume ARS solution for 30 min, and then washed with de-ionized water (DIW) after periods of 5 min with orbital shaking at 50 rpm. Samples were de-stained in 2 ml of 5% perchloric acid (chloric(VII) acid) for 15 min with orbital shaking, and absorbance was measured in triplicate in the plate reader at 405 nm and compared to an ARS-concentration standard curve. Background signal and non-extracellular matrix calcium were controlled for by including non-seeded (blank) discs. These non-seeded discs matched the material (and HAp concentration) of the seeded samples and were run along with them. Subtraction of the fluorescence reading of these blanks was used to remove the effect of scaffold staining.

Similarly, collagen deposition was measured using Sirius Red staining (SRS). The SRS solution was produced as a 1% weight-by-volume solution of Direct Red 80 (Sigma-Aldrich, UK) in 1.3% picric acid (2, 4, 6-trinitrophenol). The samples were washed in DIW after ARS, and then submerged for one hour in SRS solution under orbital shaking at 100 rpm. The staining solution was then washed out with repeated DIW after 5 min intervals of orbital shaking at 50 rpm. Each sample was then de-stained by adding 2 ml of 0.2 M NaOH:methanol and leaving in orbital shaking at 100 rpm for 20 min. Absorbance of the de-stain solution was then measured in triplicate in the plate reader at 405 nm, and compared to an SRS-concentration standard curve. Blank discs were used to control for background signal. These non-seeded discs matched the material of the seeded samples and were run along with them. Subtraction of the fluorescence reading of these blanks was used to remove the effect of scaffold staining.

2.3. Mechanical testing

The pull-to-break tensile testing protocol was followed as described in *ASTM D638-03*, in order to determine ultimate tensile strength (UTS) and elastic modulus (E). Tensile bar specimens were manufactured according to this same standard (figure 1(i)). They were subject to an elongation of 1 mm min^{-1} (recommended for smaller specimens) until fracturing occurred. Tensile testing was conducted on an LRX universal Testing Machine (Lloyd Instruments). As per the standard, five samples were tested ($n = 5$).

2.4. Thermal and molecular weight analysis

Thermal properties of the materials at different stages of the production process were analyzed using a Diamond TG/DTA scanning calorimeter (Perkin Elmer). For testing, samples of around 10 mg of the material were loaded into 40 μl aluminium sample pans. Testing temperature was held at 40 °C for 1 min in order to stabilize the starting conditions. Thermal scanning was then conducted at 10 °C minute^{-1} up to 500 °C, with a sampling rate of about 4.3 measurements per second. Polymer crystallinity (Cr) was estimated through enthalpy measurements [39, 56–58], such that:

$$Cr = \frac{\Delta H_f - \Delta H_c}{\Delta H_{100}}\% \quad (1)$$

Where ΔH_f is the fusion enthalpy, ΔH_C is the crystallisation enthalpy, and ΔH_{100} is a known value for fusion enthalpy for a fully crystalline lattice of the material in question. For PLA, this value is reported to be 91.3 J g^{-1} [59, 60].

2.5. Composite HAp concentration and distribution

As the TG/DTA process also registers gravimetric data along with the rest of its measurements, it is possible to approximate the amount of HAp contained in a composite sample after the polymer decomposes from 300 °C to 400 °C. HAp is unaffected at these temperatures, and thus should remain in the sample pans at the end of the run, and be detectable as a plateau in the weight measurements [61]. These data were obtained in triplicate for each step of the composite production process: pure PLA filament, pre-extrusion composite mixture, 3D-printing composite filament, and 3D-printed composite.

In order to examine the homogeneity of HAp distribution within the polymer matrix, we utilised a FEI Inspect F50 Scanning Electron Microscope (SEM) with Electron Dispersive Spectroscopy (EDS) module. Scanning Electron Microscopy with Electron Dispersive Spectroscopy (SEM-EDS) was performed on cross-sections of 3D-printed samples from each production step to observe their elemental composition and distribution. Additionally, micro Computed

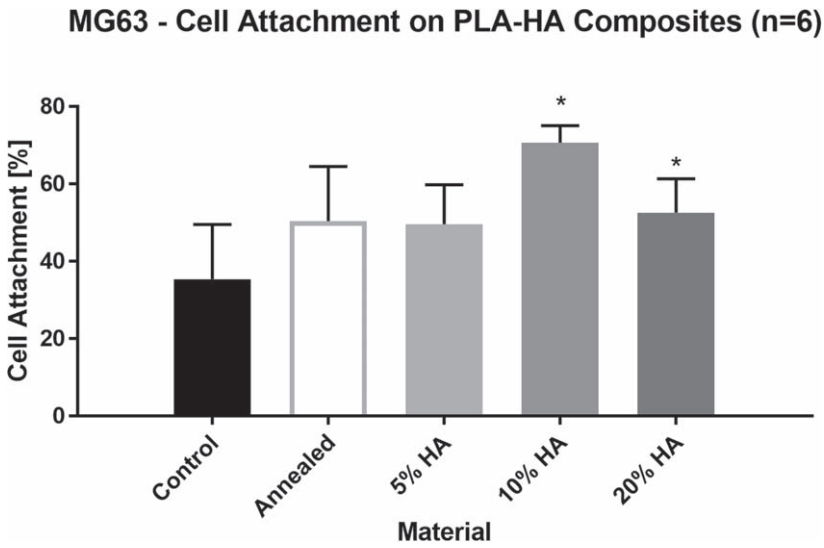

Figure 2. MG63 cell-line attachment on 3D-printed discs of different PLA composites. Cell attachment mean ± S.D was calculated as the proportion of cells as measured by their metabolic activity remaining on the samples versus those remaining in the incubation wells. * = significantly different ($p<0.05$) from pure-PLA control discs; n = 6 from triplicate samples on two biological repeats.

Tomography (μCT) using a Skyscan 1172 High Resolution Micro-CT (Bruker microCT). Imaging was done at a voltage of 50 kV, 180° rotation, and exposure of 1210 ms. These imaging data were used to produce 3D reconstructions of the volumetric distribution of ceramic particles within a 3D-printed specimen.

In order to assess the effects of processing in the molecular structure of the polymer matrix, we analyzed samples throughout the production process using Gel Permeation Chromatography (GPC) in a 1090 HPLC equipped with UV–vis and Differential Refractive Index Detectors (Hewlet-Packard, UK). For each stage of the production process, triplicate samples of 10 mg of material were dissolved in chloroform to 0.10 mg ml^{-1}, and were then subjected to GPC, with results reported as calibrated against a polystyrene standard.

2.6. Statistical analysis

Data for these experiments was processed and analysed using Graphpad Prism 7.03. Data gathered through several time points (such as 23-day cell culture assays) was compared through Two-Way ANOVA with Sidak hypothesis testing for multiple comparisons. Data gathered on a single time point (such as collagen and calcium deposition) was compared through One-Way ANOVA with Tukey hypothesis testing for multiple comparisons. Significance level was defaulted to $p > 0.05$; this value is also clarified for each experiment.

3. Results

3.1. Material biocompatibility *in vitro*

The MG63 cell line grew well on all tested materials under the conditions of this study (figure 2). In terms of cell attachment, the 10% HAp and 20% HAp composites supported higher initial cell numbers with respect to the control PLA ($p < 0.05$). The 10% HAp composite was significantly more favourable for attachment than the 20% HAp version ($p < 0.05$).

Cell viability (metabolic activity) increased over time in all samples (figure 3) and there were only significant differences ($p < 0.05$) at day 14, when the 5% HAp and 20% HAp PLA composites supported lower cell numbers than the other materials. These differences were not observable by day 21, but all samples reached significantly higher cell counts ($p < 0.05$) than the reference tissue culture plastic (TCP).

3.2. The ability of the materials to support matrix deposition and mineralisation

MG63 calcium deposition over 23 days on the sample discs was slightly but significantly higher in the 5% HAp and 20% HAp composites with respect to pure PLA controls ($p < 0.05$) (figure 4). However, only the 20% HAp composite supported higher collagen deposition than the TCP reference group ($p < 0.05$).

3.3. Composite characterisation

3.3.1. Composite selection

The 10% HAp composite was found to be pose less problems during extrusion and 3D-printing—this was the main reason for the final decision in favour of this formulation. Moreover, the cell culture tests indicated it supported cells as well as the other composite versions by the end of the trial period, and also performed marginally better for cell-attachment. Further characterisation was thus performed on specimens of the 10% HAp composite only. Pure PLA samples were tested as a base reference, and annealed

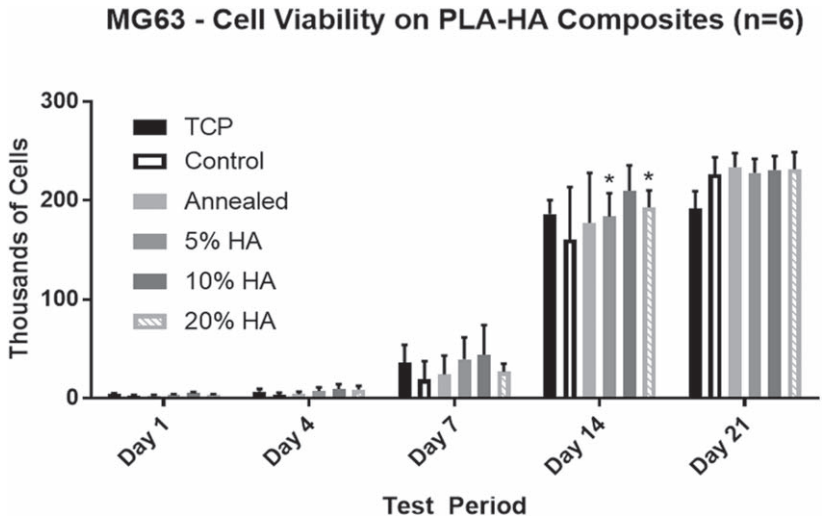

Figure 3. MG63 cell-line viability results observed over 21 on 3D-printed discs of the PLA variants studied. Stars denote significant differences ($p = 0.05$) from the pure PLA control group. TCP measurements are included as a reference for baseline cell-line viability. * = significantly different ($p = 0.05$) from pure-PLA control discs; n = 6 from triplicate samples on two biological repeats.

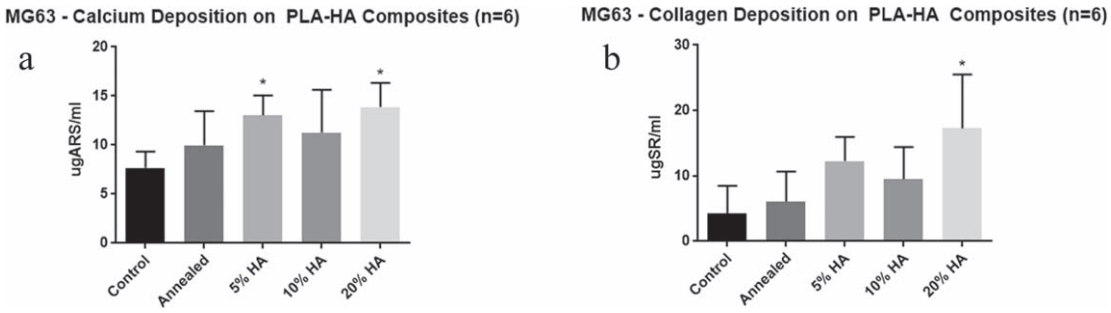

Figure 4. (a) MG63 cell-line calcium and (b) collagen deposition over 23 days on the PLA variants studied. Presence of both substances was evaluated through ARS and SRS essays, respectively. * = significantly different ($p = 0.05$) from pure-PLA control discs; n = 6 from triplicate samples on two biological repeats.

PLA was tested to assess any effects of changes in crystallinity.

3.3.2. Mechanical testing

Mechanically (figure 5(a)), the composite was found to have lower UTS (28.65 MPa) than non-annealed PLA (48.46 MPa) and similar to annealed PLA tensile bars (27.74 MPa). This meant that both annealed and composite samples were about 40% weaker than pure PLA controls. There were no significant differences between the 10% HAp composite and the annealed material ($p < 0.05$).

Elastic modulus was very similar between pure PLA (202.4 kPa) and the annealed tensile bars (178.9 MPa), the difference being non-significant ($p < 0.05$) (figure 5(b)). However, elastic modulus of the 10% HAp composite (126.5 MPa) was significantly lower than that of pure PLA ($p < 0.05$).

3.3.3. Thermal analysis and HAp distribution

Polymer crystallinity values were calculated from differential calorimetry through equation 1 (figure 6(a)). Only annealing showed a significant effect on the raw material's crystallinity value, increasing it by 66% with respect of the raw PLA filament ($p < 0.05$). Neither 3D-printing nor melting for composite production, nor extrusion into composite filament had a significant effect on the material's original crystalline content ($p < 0.05$). Moreover, 3D-printed parts from both raw and composite filaments showed no significant difference compared to each other ($p < 0.05$). In terms of molecular weight, the material remained consistent through processing before 3D-printing. The combination of further heating and the pressure from extrusion during printing likely provide enough energy to cause the significant lowering on molecular weight observed (figure 6(c)). In turn, this could explain the lowering of elasticity and tensile strength mentioned above (figure 5).

The HAp content of the analyzed samples at the three consecutive stages of the composite filament production process was measured through TGA (figure 6(b)). This reflects the ceramic left over after polymer matrix decomposition during calorimetry.

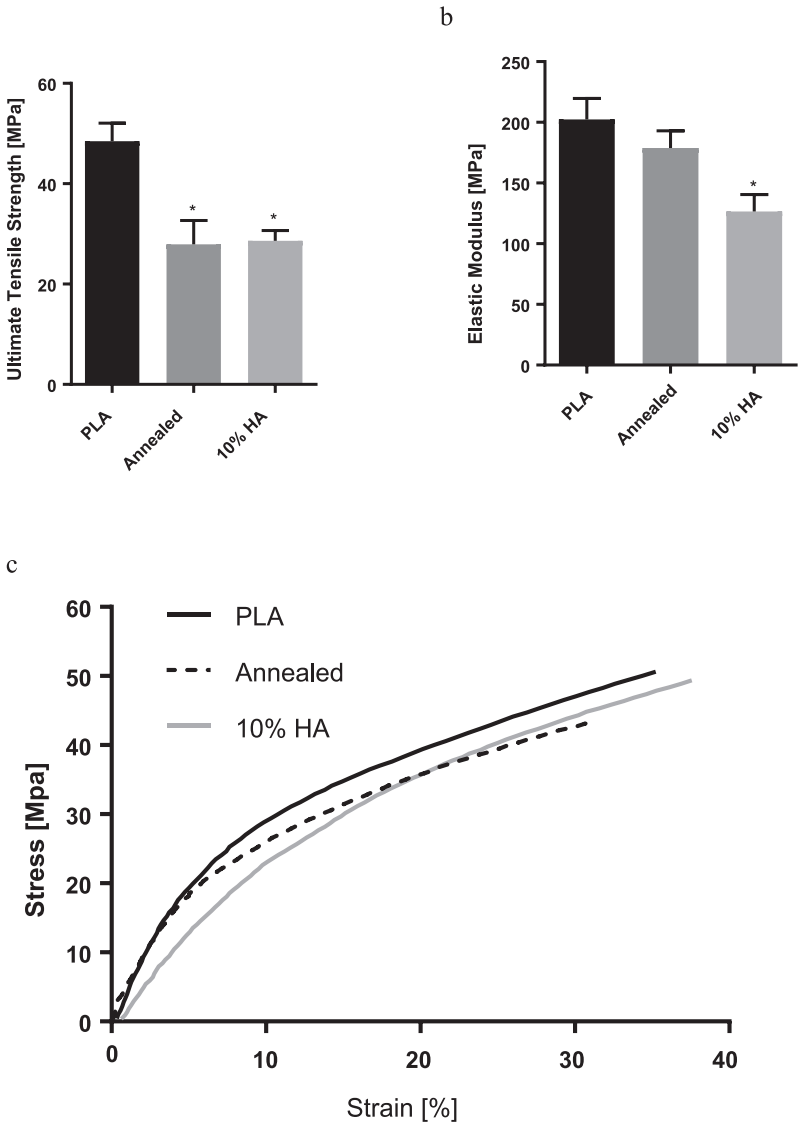

Figure 5. (a) Tensile strength and (b) elastic modulus measurements for pure PLA (as control group), annealed PLA, and the 10% HAp composite used in this study. (c) Representative stress-strain yield curves for one sample of each of the materials. Pull-to-break testing was conducted on 3D-printed tensile bars ($n = 5$), both with specifications as per *ASTM D638-03*. * = significantly different ($p < 0.05$) from pure-PLA samples; n = 5.

There was no statistical difference between the pre-extrusion composite, the extruded filament, or the 3D-printed parts made of the 10% HAp composite ($p < 0.05$). An average of 7%-by weight-HAp content was found throughout the whole process, being lower than the 10%-by-weight used when mixing the raw components, with wider dispersion of the data after the initial melting into the composite disc. SEM-EDS images of cross-sections of filament and 3D-printed samples demonstrated uniform distribution of Ca and P atoms (figures 7(c), (d), (h), (i)) on the analysed area, with the O atoms' distribution (figure 7(c)) shown as a reference for the PLA matrix, which dominates as expected. Characteristic peaks for Ca and P were found in all samples except the pure PLA one. The most defined peaks for Ca and P appeared in the 3DP composite filament, and the 3D-printed composite specimens (figures 7(b), (g)). EDS data is presented qualitatively, since the facture surface analysed could not be completely flattened and smoothed: both factors were considered to affect elemental quantification. Additionally, the scanned surfaces (especially those on the 3D-printed sample) showed numerous zones of charge artefacts, thus the analysed area's irregular geometry was selected so as to cover the largest possible section of artefact-free image.

The behaviour of the materials under differential calorimetry was as expected for PLA, (figure 9). The changes in crystallinity mentioned above are apparent in these curves, with the most notable variation being the obliteration of the crystallization peak on the pre-extrusion composite disc—along with its re-appearance after extrusion into a 3D-printing filament. Additionally, melting for composite production appeared to induce an increase in heat capacity on the polymer's structure, inferred from the offset of its curves along

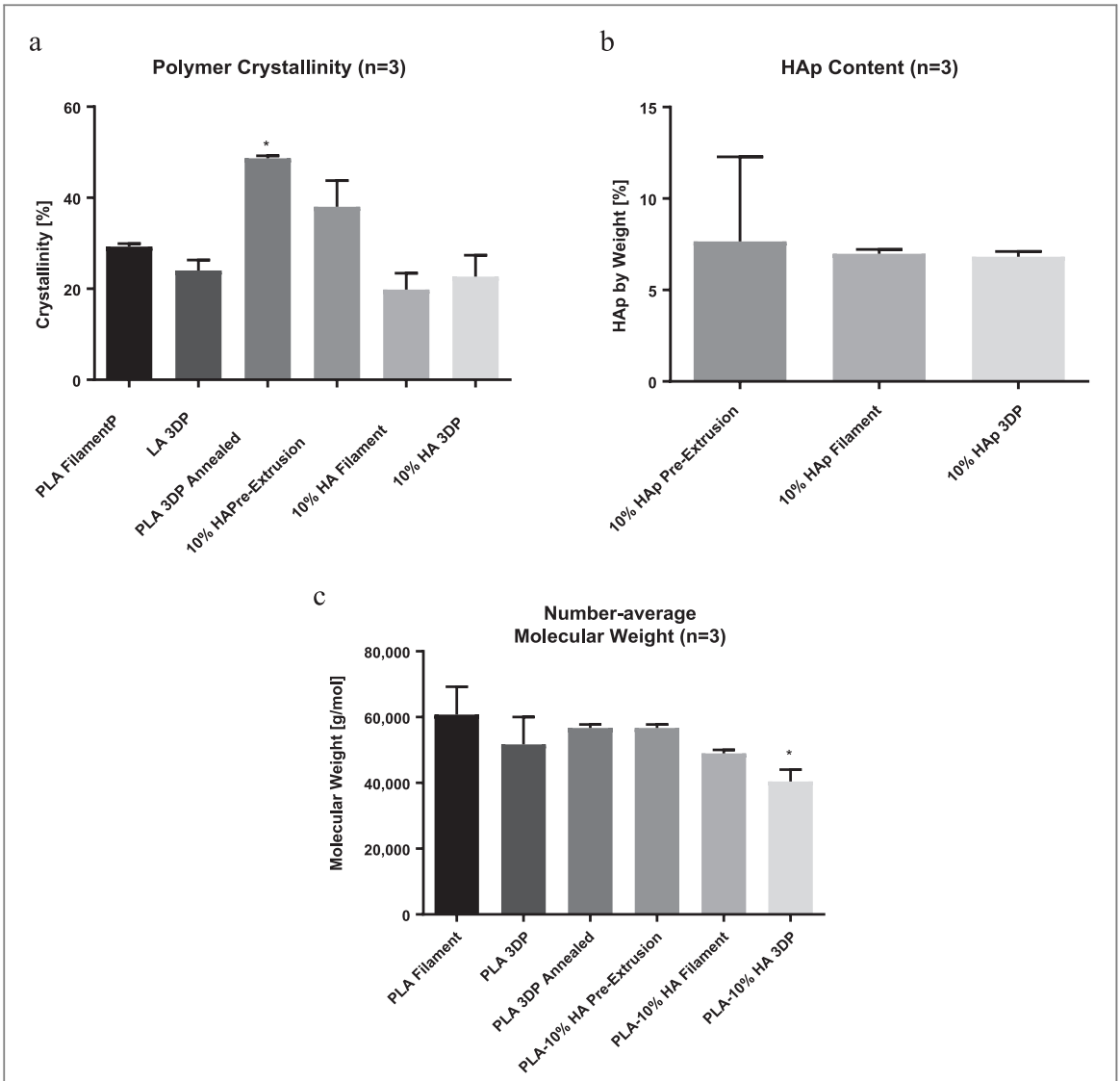

Figure 6. (a) Percent crystalline content after different processing stages for PLA; from left to right, bars correspond to: the 3D-printing filament used as raw material for this study; raw material after being 3D-printed; 3D-printed material after annealing; 10% HAp composite disc before feeding to the Filabot extruder; the output 10% HAp composite filament from the extruder; and the 10% HAp composite filament after being 3D-printed. (b) HAp content in the composite variants tested; bars correspond to the last three materials of figure 6(a). (c) Number-average molecular weight measurements corresponding to the same materials as in (a). * = significantly different ($p = 0.05$) from pure-PLA samples; n = 3.

the heat-flow axis. Extrusion, on the other hand, yields a small difference in this respect, while 3D-printing pushes a further increase. Notably, 3D-printing of the raw filament did not produce any large effect on heat capacity—the curve is not shown as it closely overlaps with that of the raw material. The average melting temperature for the 3D-printed composite (~174 °C) was significantly lower than for the other materials ($p < 0.05$).

Reconstruction through μCT of a 3D-printed disc like those mentioned for cell culture (figure 1(c)) revealed an uniform distribution of microscopic radiopaque particles on the outermost surfaces of the sample (figure 8(a)). These can be seen in the images as uncountable lighter spots interposed with darker, more radiolucent polymer matrix. Adjusting the reconstruction parameters to exclude low-opacity sections of the images, it was possible to produce an 3D mapping of the distribution of what appears to be HAp particles. This volumetric dispersion was consistent with SEM-EDS observations.

4. Discussion

The results presented here address gaps in our knowledge regarding the biological properties of 3D-printed PLA, as well as its implementation as a composite for FFF– which has not been thoroughly studied. PLA is currently deemed safe for clinical use, a claim firmly supported in the literature [30, 31, 38, 39, 62–64]. The aim of this study and the on-going research behind it is to develop viable solutions for bone-regeneration applications, implemented through additive manufacturing. As a newer fabrication process, FFF in the context of therapeutics has only recently received

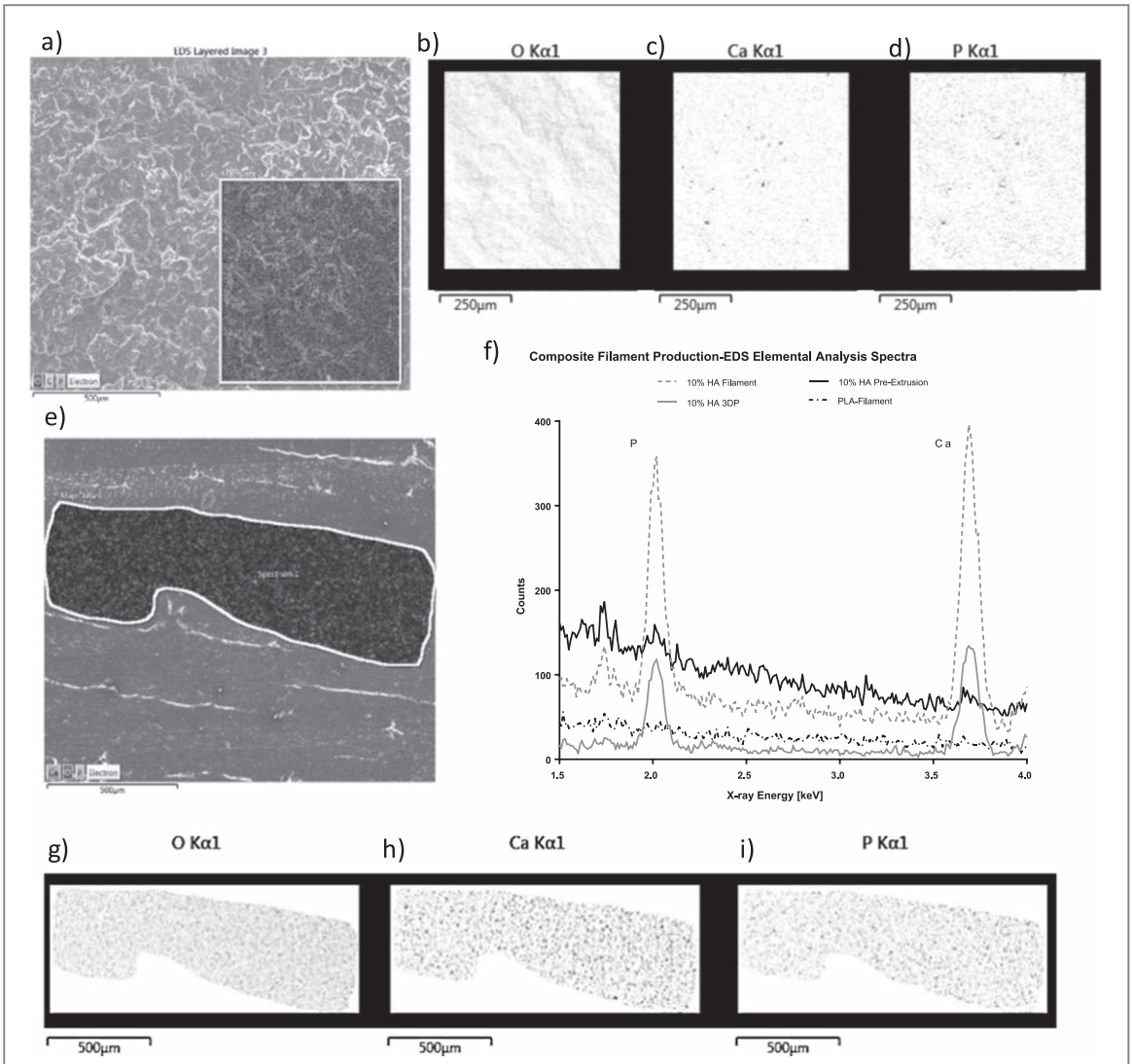

Figure 7. SEM-EDS images of 3D-printed PLA-10%HAp composite. (a) SEM image of transversely cut PLA-10%HAp filament scanned at 20 kV. The filament's polymer matrix's distribution of (b) oxygen, (c) calcium and (d) phosphorous were detected. (e) SEM image of transversely cut 3D-printed PLA-10%HAp scanned at 20 kV. (f) Elemental spectral analysis of the PLA-10%HAp composite production stages, from top to bottom at 1.5 keV, curves correspond to pre-extrusion composite, composite filament, pure PLA filament, and 3D-printed composite. EDS was performed on the highlighted area of the SEM image to analyze for elemental signals of HAp. The 3D-printed polymer matrix's distribution of (g) oxygen, (h) calcium and (i) phosphorous were detected.

more attention in academic publications. Although there is little reason to believe 3D-printing could affect the safety of PLA and HAp, custom implants with biological inductors will foreseeably be classified as Class III medical device, and will therefore be required to adhere to good manufacturing practices. As such, strong evidence must be produced to support the biological safety of 3D-printing in the production of polymer-based composite implants [65].

Here we have shown that *in vitro* biocompatibility is clearly unaffected in 3D-printed materials made with commercial-grade PLA. Though metabolic activity may not remain constant per-cell during these kinds of experiments, RRA is generally accepted as an indirect measure of cell growth, as increase in metabolic activity alone is unlikely to yield readings increasing several orders of magnitude [66]. We have also provided evidence that these materials perform similarly to tissue culture plastic in terms of supporting cell metabolic activity which is an indicator of viability. With respect of the 10% HAp formulation we selected, at least one more group has reached a similar formulation for PLA-HAp composite for 3D-printing [7], but yet others have been successful with formulations of up to 50% HAp [6, 9]. Differences in raw materials between results in this and the cited studies are likely the culprits behind the range of viable formulations for compositing PLA-HAp for FFF. It has been pointed out for similar polymer-ceramic composites that the main benefit of ceramic particulates comes from increased surface roughness enhancing cell-attachment [14], which might be the mechanism behind increased cell-attachment measurements in composites when compared to pure PLA and the lowest concentration (5% HAp) we evaluated. Given that surface roughness influences cell attachment, but cell proximity is necessary for long term survivability, we hypothesize that the significant differences favouring

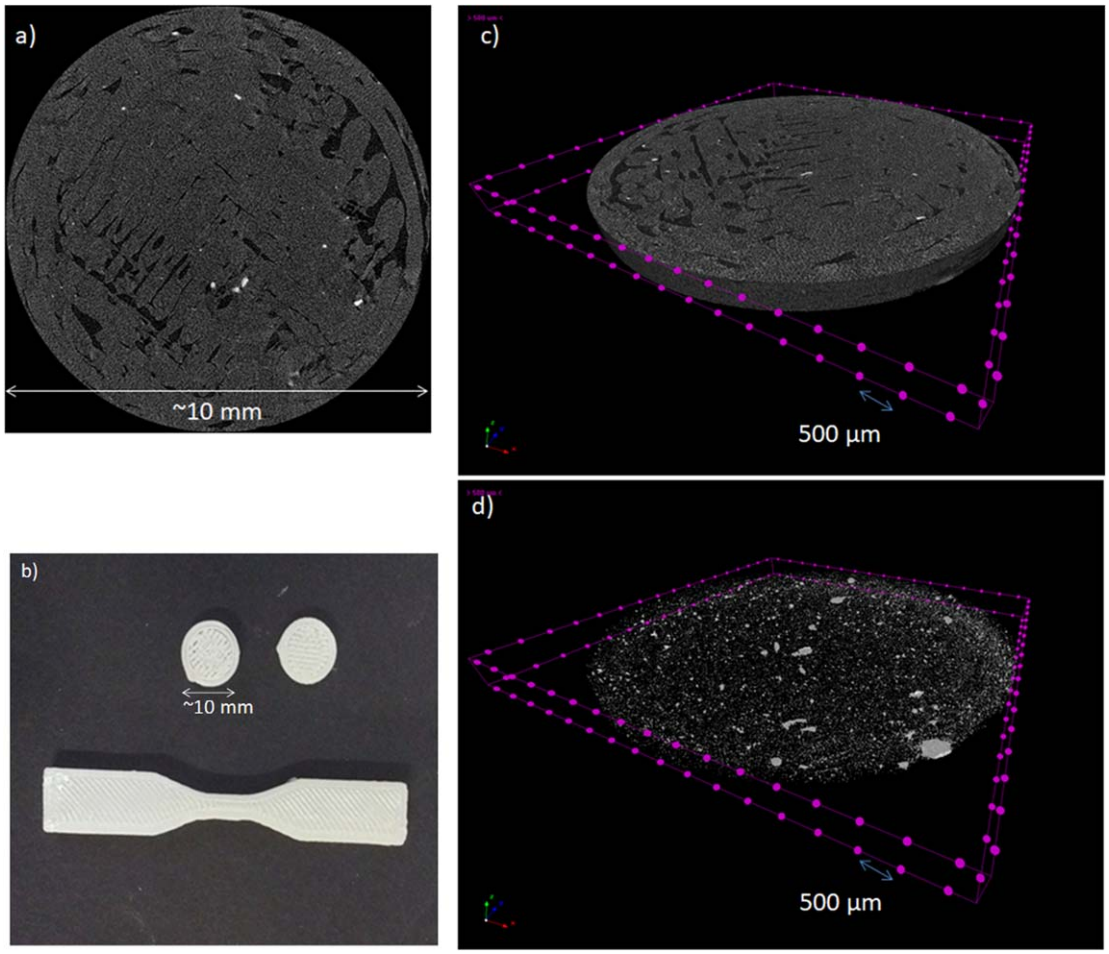

Figure 8. μCT images of 3D-printed disc made with PLA-10%HAp composite. (a) Uppermost axial projection image of a 1 cm disc sample; (b) photograph of 3D-printed sample disc shown in relationship to a 3D-printed tensile bar specimen; (c) 3D reconstruction of the sample's volume using 2 μm slice thickness; (d) 3D reconstruction of the sample's volume with reconstruction parameters adjusted to filter out the more radiolucent material: the remaining particles shown are assumed to correspond to HAp.

attachment to the 10% HAp composite over the 20% HAp version might arise from the former producing more consistent surfaces during 3D-printing. This would allow cells to also attach more consistently and uniformly and would account for the wider standard deviation seen for the 20% HAp.

As it is usually pointed out in the literature, normal biological and physical degradation of PLA produces no by-products other than lactic acid, which is readily metabolized, and will only accumulate to cause inflammatory responses over long periods of stagnation [67, 68]. *In vitro*, the mechanisms to cope with lactic acid leachate from the samples are likely to be similar to *in vivo* vascular drainage, since culture medium is regularly changed. Relevant to this *in vitro* setting, osteosarcoma cells—such as the MG63 cell-line—have been found to express MCT receptors, including MCT-1, which facilitates lactic acid uptake [69]. It is therefore likely that cells in the tissue culture wells dispose of excess lactic acid through their own metabolism, while the as-per-protocol culture medium changes and well washes during the study do not allow for an unmanageable build-up of the by-product.

The creation of a composite with PLA and HAp as a means to promote bone regeneration has been based on the fact that HAp has been documented to enhance repair in bone lesions by favouring overall osteointegration of implants [14, 42, 70–73]. Coupled with the biocompatibility and bioresorbability of PLA, such a material could yield numerous benefits in complex skeletal-repair situations, such as reconstruction of facial structures in growing children—in whom it is desirable for implant materials to resorb quickly to prevent craniofacial malformation. In this study we have documented a general production method for a 3D-printing composite filament. Previous research in similar compositing for electro-spinning suggested that—in terms of *in vitro* cell response—the ideal amount of HAp in a polymer mix was somewhere below 10% as an additive for electrospinning (another additive manufacturing technique) [74], while other studies in FFF have found printable blends of up to 50% HAp with favourable cell response [6, 7, 9]. In this study, the results for 20% HAp concentrations suggests that higher concentrations of HAp have benefits on the biological response. However, considering

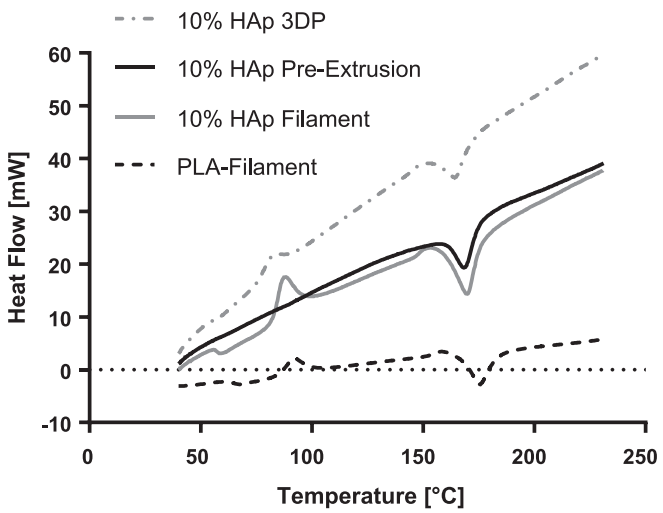

Figure 9. Differential calorimetry curves for the studied PLA-HAp composite through its production stages. The usual crystallization peaks for PLA can be observed at around 90 °C, with melting peaks near 180 °C. From top to bottom curves, average melting peaks for each material ($n = 3$) were observed at 174.8 °C, 176.0 °C, 176.8 °C, and 175.8 °C. Endothermic processes are arbitrarily depicted downwards.

that all measurements except collagen deposition were similar for all concentrations of HAp, these benefits may not improve significantly with further increasing the HAp content of the material. In the case of 10% HAp,

Moreover, increasing HAp concentration rapidly becomes problematic for material processing and printing. Extruding and 3D-printing the 20% HAp composite proved to be more challenging that for the 10% HAp under the conditions described here. During extrusion into filament, uniform flow of the softened polymer was prohibitively difficult to achieve. This resulted in persistent and unavoidable imperfections on the surface of the resulting filament, along with naked-eye-noticeable inconsistencies in its diameter. These irregularities make it hard for the 3D-printer to produce optimal-quality prints, and eventually result in either fracture of the filament, or clogging of the printer's extruding mechanisms within minutes—seemingly via accumulation of HAp in the channel leading from the heating chamber to the nozzle. The 5% and 10% HAp composites showed no such problems with filament extrusion, though printer blockage did occur after several hours of use of these filaments.

The higher concentration of HAp in the 20% HAp composite probably allows for the powder to agglomerate during the melting phase of the compositing process. These HAp agglomerates could then consolidate further under the pressure of the driving screw during extrusion, which is likely to produce the 250 MPa required for cold isostatic pressing of HAp [75]. Given the larger agglomerates of ceramic observed in figure 8(d), we theorize that improving the uniformity of the HAp powder dispersion on the polymer before melting could potentially resolve this issue (by preventing these agglomerates from forming), but that would require grinding the PLA pellets further, or the use of a solvent to thoroughly homogenize the mixture. The Filabot extruder requires the pellets be large enough for the driving screw to force them in to the melting chamber; as such, there is a limit to the pellet size suitable to use for this device (which is likely around 3 mm, as the device was designed to accept commercial plastic pellets); commercial-size granules would likely not be extrudable with this device. Alternatively, using a solvent poses several biological safety issues, mainly the difficulty of assuring it has been completely evaporated during extrusion and printing, especially since the composite is meant for resorbable implants—the production method here presented was designed purposefully to avoid the use of solvents. Moreover, the amount of solvent required to process hundreds to thousands of grams of PLA would be costly and problematic with regards to disposal.

For the former reasons, under the conditions of this study, the 20% HAp composite was deemed unsuitable to use, despite it showing a tendency to encourage the deposition of collagen on the MG63 cell-line. The remaining two composite concentrations showed no further differences, except for the significantly better *in vitro* cell attachment properties of the 10% HAp composite. Overall, ease of manufacturing was the main reason this version of the composite was favoured for the remainder of this study. We do not completely discard the possibility that further *in vitro* testing may provide evidence in favour of higher concentrations, which would require refinement of our production methods.

The addition of this relatively small amount of HAp to the PLA polymer matrix was not expected to impact on the overall mechanical properties of the printed parts. Other studies on PLA-ceramic composites for FFF have found an increase in mechanical properties with no change on the *in vitro* degradation profile of the material in simulated bodily fluids at 37 ° C [14]. This is not surprising, since *in vitro* degradation of PLA at physiological temperatures has consistently been found to happen over months to years [76–78]. It is worth mentioning that the mechanical properties for this material are low compared to usual values for PLA manufactured through other processes [38, 79–81], but our proposed application in facial reconstruction is aimed at non-load bearing sections of the skull, and thus mechanical properties a not considered critical. The filament production processes, on the other hand, were a concern in this respect, as they involve several cycles of melting and cooling. The significant drop in tensile strength and elastic modulus found in 3D-printed samples with the 10% HAp composite could be explained as being a reflection of increased crystallinity, but no significant difference was found compared to the reference 3D-printed PLA. Annealed PLA tensile bars produced through 3D-printing showed a similarly lowering tensile strength, along with an increase in crystallinity, with elasticity remaining similar to the reference material. This suggests that increased crystallinity may not be the main factor affecting mechanical resistance on this composite.

Other research has found that PLA-HAp composites (produced through hot pressing) achieve higher tensile strengths and elastic moduli, probably due to the superposition of the mechanical properties of both materials [45]; those composites were prepared through mixing in solvent, and with a much higher HAp concentration (70% to 85% by weight). The same mechanisms might not apply to the present production methods—even though thorough dispersion of HAp is achieved—due to the concentrations allowed by this study's methods being much lower. The layer-layer interface in 3D-printed parts is also proposed to counter whatever benefits HAp compositing brings to the material, since they 3D-printing results in lower tensile strengths than those found moulded or pressed PLA [76, 79, 82, 83].

Further insight on this phenomenon could arise from analyzing the molecular weight of the polymer during processing, as repeated melting under a non-dry atmosphere could potentially degrade it, explaining the compromise on its mechanical properties [76, 78, 84–87]. The lower concentration of HAp could also mean that the ceramic particles are simply embedded within the polymer matrix, interrupting intermolecular interactions between PLA chains, and thus accounting for part of the lowering of mechanical properties.

Likewise, the lowering of melting peak observed for the composite after 3D-printing is likely reflective of lowering of the molecular weight of the polymer matrix due to repeated thermal treatments during processing—this would, in turn, weaken the mechanical resistance of the final samples. The resulting upward shift in the calorimetry curves could be the result of intermolecular interactions with hydroxyl moieties provided by the presence of HAp [88], which could potentially facilitate hydrogen bonding to account for the heightened heat capacity at the compositing stages before 3D-printing. Furthermore, the self-reinforcing phenomenon [89] could also be a potential explanation for the second shift happening after 3D-printing, since polymer-chain alignment could further favour intermolecular interactions with HAp particles, and likely strengthen them through reorientation into more favourable bonding angles on a more tightly packed matrix.

5. Conclusions

We present here a method for producing a PLA-HAp composite 3D-printing filament for the production of implantable, resorbable devices for bone regeneration in the context of maxillofacial reconstruction. PLA is used as an inert structural material to which HAp particles are added solvent-free as a functionalizing agent to promote osteoconduction and osteoinduction. This composite filament allows for free-form-fabrication in commercial-grade 3D-pritners, and has the potential to be used in the treatment of complex bone defects and lesions where standardized plates, screws, and autologous implants are geometrically or mechanically sub-optimal. Our evidence suggests that the process is biologically safe, and—in the mid-term—would require minor adjustments (such as sterilizing the filament extruder and 3D-printer) to move forward to *in vivo* testing for biocompatibility, bone-regeneration capabilities, and implant degradation.

Acknowledgments

The authors would like to thank The University of Sheffield (United Kingdom) and the National Council for Science and Technology (CONACyT, Mexico, grant No. 384699) for co-funding this research. We also extend our gratitude to the School of Clinical Dentistry, the Department of Materials Science and Engineering, and the Insigneo Institute for *in silico* Medicine—all at The University of Sheffield—for their support in the form of research staff and facilities.

ORCID iDs

C Amnael Orozco-Díaz https://orcid.org/0000-0001-9095-3857
Robert Moorehead https://orcid.org/0000-0001-6608-9384

Gwendolen C Reilly https://orcid.org/0000-0003-1456-1071
Fiona Gilchrist https://orcid.org/0000-0002-0418-6274
Cheryl Miller https://orcid.org/0000-0002-6062-6254

References

[1] Stoor P *et al* 2014 Rapid prototyped patient specific implants for reconstruction of orbital wall defects *J. Cranio-Maxillofacial Surg.* **42** 1644–9
[2] Hughes C W *et al* 2003 The custom-made titanium orbital floor prosthesis in reconstruction for orbital floor fractures *Br. J. Oral Maxillofac. Surg.* **41** 50–3
[3] Birkenfeld F *et al* 2013 Forces affecting orbital floor reconstruction materials-A cadaver study *J. Cranio-Maxillofacial Surg.* **41** e24–8
[4] Kantaros A, Chatzidai N and Karalekas D 2016 3D printing-assisted design of scaffold structures *Int. J. Adv. Manuf. Technol.* ed Y Moreno 82 6th ed. (London: Springer-Verlag) 559–71
[5] Coelho C P G *et al* 2018 Osteogenic effects of dipyridamole versus rhBMP-2 using 3D-printed bioceramic scaffolds in a growing alveolar cleft model presenter *Plastic and Reconstructive Surgery, Global Open* **6** 133–134
[6] Corcione C E *et al* 2017 3D printing of hydroxyapatite polymer-based composites for bone tissue engineering. *Journal of Polymer Engineering* **37** 741–6
[7] Niaza K V, Senatov F S, Kaloshkin S D *et al* 2016 3D-printed scaffolds based on PLA/HA nanocomposites for trabecular bone reconstruction *J. Phys. Conf. Ser. [Internet].* **741** 012068
[8] Jardini A L *et al* 2014 Cranial reconstruction: 3D biomodel and custom-built implant created using additive manufacturing *J. Cranio-Maxillofacial Surg.* **42** 1877–84
[9] Esposito C *et al* 2018 One-step solvent-free process for the fabrication of high loaded PLA / HA composite filament for 3D printing *J. Therm. Anal. Calorim. [Internet].* **134** 575–82
[10] Shao H *et al* 2017 3D robocasting magnesium-doped wollastonite/TCP bioceramic scaffolds with improved bone regeneration capacity in critical sized calvarial defects *J. Mater. Chem. B.* **5** 2941–51
[11] Khojasteh A *et al* 2017 Guided bone regeneration for the reconstruction of alveolar bone defects *Ann. Maxilofac. Surg. J* **7** 263–77
[12] Mazzoni S *et al* 2015 Computer-aided design and computer-aided manufacturing cutting guides and customized titanium plates are useful in upper maxilla waferless repositioning *J. Oral Maxillofac. Surg. [Internet].* **73** 701–7
[13] Eggbeer D *et al* 2012 Evaluation of direct and indirect additive manufacture of maxillofacial prostheses *Proc. Inst. Mech. Eng. Part H-Journal Eng. Med* **226** 718–28
[14] Melo P *et al* 2019 Osteoinduction of 3D printed particulate and short-fibre reinforced composites produced using PLLA and apatite-wollastonite *Compos. Sci. Technol. [Internet].* **184** 107834
[15] Rohner D *et al* 2013 Importance of patient-specific intraoperative guides in complex maxillofacial reconstruction *J. Cranio-Maxillofacial Surg. [Internet].* **41** 382–90
[16] Nyberg E L *et al* 2017 3D-printing technologies for craniofacial rehabilitation, reconstruction, and regeneration *Ann. Biomed. Eng.* **45** 45–57
[17] Ologunde R and McLeod N M H 2018 Use of patient-reported outcome measures in oral and maxillofacial trauma surgery: a review *Br. J. Oral Maxillofac. Surg. [Internet].* **56** 371–9
[18] Ross R B 1987 Treatment variables affecting facial growth in complete unilateral cleft lip and palate. Part 5 [Internet] *Cleft Palate J* 5–77 Available from http://ncbi.nlm.nih.gov
[19] Kremenak C R, Huffman W C and Olin W H 1970 Growth of maxillae in dogs after palatal surgery *II. Cleft Palate J* **4** 719–36 (http://cleftpalatejournal.pitt.edu/ojs/cleftpalate/article/view/136)
[20] Eppley L 1996 Alveolar Cleft Bone Grafting Part I: Primary Bone Grafting. *Cleft Palate Journal* **54** 74–82
[21] Friede H and Johanson B 1974 A follow-up study of cleft children treated with primary bone grafting. 1 *Orthodontic aspects. Scand. J. Plast. Reconstr. Surg.* **8** 88–103
[22] Rehrmann A H, Koberg W R and Koch H 1970 Long-term postoperative results of primary and secondary bone grafting in complete clefts of lip and palate *Cleft Palate J.* **7** 206–21 (http://cleftpalatejournal.pitt.edu/ojs/cleftpalate/article/view/289)
[23] Seifeldin S A 2016 Is alveolar cleft reconstruction still controversial ? (Review of literature) *Saudi Dent. J.* **28** 3–11
[24] Lilja J 2009 Alveolar bone grafting *Indian J. Plast. Surg.* **42** 110
[25] Report C 2002 The reconstruction of bilateral clefts using endosseous implants after bone grafting. *The reconstruction of bilateral clefts using endosseous implants after bone grafting.* **121** 403–10
[26] Martin-Smith J D *et al* 2013 Repair of anterior cleft palate fistulae with cancellous bone graft *Plast. Reconstr. Surg.* **131** 380e–7e
[27] Du Y *et al* 2018 Block iliac bone grafting enhances osseous healing of alveolar reconstruction in older cleft patients: a radiological and histological evaluation 23
[28] Eppley L 1996 Alveolar Cleft Bone Grafting Primary (Part I): Primary Bone Grafting. **54** 74–82
[29] Ochs M W and Ii P 1996 Alveolar cleft bone grafting part II: secondary bone grafting *Cleft Palate J.* 83–8
[30] Liebert M A *et al* 2005 Biocompatibility of bioresorbable Poly (L-lactic acid) composite scaffolds obtained by supercritical gas foaming with human fetal bone *Tissue Engineering* **11** 1640–9 (https://www-liebertpub-com.sheffield.idm.oclc.org/doi/pdf/10.1089%2Ften.2005.11.1640)
[31] Bergsma J E *et al* 1995 In tivo degradation and biocompaGbility study of in vitro polylactide particles. *Biomaterials* **16** 267–74
[32] Haug R H, Nuveen E and Bredbenner T 1999 An evaluation of the support provided by common internal orbital reconstruction materials *J. Oral Maxillofac. Surg.* **57** 564–70
[33] Cordewener F W *et al* 1996 Poly(L-lactide) implants for repair of human orbital floor defects: clinical and magnetic resonance imaging evaluation of long-term results *J. Oral Maxillofac. Surg.* **54** 9–13 discussion 13-4
[34] Kantaros A, Chatzidai N and Karalekas D 2015 3D printing-assisted design of scaffold structures *Biomaterials* **16** 559–71
[35] Gosau M *et al* 2011 Retrospective analysis of orbital floor fractures-complications, outcome, and review of literature *Clin. Oral Investig.* **15** 305–13
[36] Chia H N and Wu B M 2015 *Recent advances in 3D printing of biomaterials.* **9** 1–14
[37] Vert M *et al* 1992 Bioresorbability and biocompatibility of aliphatic polyesters *J. Mater. Sci., Mater. Med.* **3** 432–46
[38] Athanasiou K A, Niederauer G G and Agrawal C M 1996 Sterilization, toxicity, biocompatibility and clinical applications of polylactic acid/polyglycolic acid copolymers *Biomaterials* 17
[39] Henton D E *et al* 2005 Polylactic acid technology *Nat. Fibers, Biopolym. Biocomposites.* **12** 527–78
[40] Majola A *et al* 1992 Absorbable self-reinforced polylactide (SR-PLA) composite rods for fracture fixation: strength and strength retention in the bone and subcutaneous tissue of rabbits *J. Mater. Sci., Mater. Med.* **3** 43–7
[41] Koskikare K *et al* 1996 Intraosseous plating with absorbable self-reinforced poly-L-lactide plates in the fixation of distal femoral osteotomies on rabbits *J. Biomed. Mater. Res.* **30** 417–21
[42] Wu F *et al* 2012 Premixed, injectable PLA-modified calcium deficient apatite biocement (cd-AB) with washout resistance *Colloids Surfaces B Biointerfaces.* **92** 113–20
[43] Russias J *et al* 2006 Fabrication and mechanical properties of PLA/HA composites: a study of *in vitro* degradation *Materials Science and Engineering C* **26** 1289–95

[44] Tanodekaew S, Channasanon S and Kaewkong P 2013 PLA-HA scaffolds : preparation and bioactivity *Procedia Eng. [Internet].* **59** 144–9
[45] Russias J *et al* 2015 Fabrication and mechanical properties of PLA/HA composites: a study of *in vitro* degradation *Mater. Sci. Eng. C* **26** 1–15
[46] Wei G and Ma P X 2004 Structure and properties of nano-hydroxyapatite/polymer composite scaffolds for bone tissue engineering *Biomaterials* **25** 4749–57
[47] Warabino K, Ueno S and Hino T 2006 Preperation and adsorption properties of hydroxyapatite surface-modified by cetylphosphate *Phosphorous Research Bulletin* **20** 129–34
[48] Zhu W *et al* 2010 Experimental study on the conduction function of nano-hydroxyapatite artificial bone *Micro Nano Lett. [Internet].* **5** 19
[49] Prakash K H *et al* 2006 Apparent solubility of hydroxyapatite in aqueous medium and its influence on the morphology of nanocrystallites with precipitation temperature *Langmuir* **22** 11002–8
[50] Chang B S *et al* 2000 Osteoconduction at porous hydroxyapatite with various pore configurations *Biomaterials* **21** 1291–8
[51] Senatov F S *et al* 2016 Low-cycle fatigue behavior of 3d-printed PLA-based porous scaffolds *Compos. Part B [Internet].* **97** 193–200
[52] Alharbi N *et al* 2015 Processing of apatite-wollastonite (AW) glass-ceramic for three dimensional printing (3DP) *Appl. Mech. Mater.* **754–755** 974–8
[53] Shao H *et al* 2016 3D printing magnesium-doped wollastonite/β-TCP bioceramics scaffolds with high strength and adjustable degradation *J. Eur. Ceram. Soc. [Internet].* **36** 1495–503
[54] Zocca A *et al* 2015 3D-printed silicate porous bioceramics using a non-sacrificial preceramic polymer binder *Biofabrication* 7
[55] Shao H *et al* 2018 Custom repair of mandibular bone defects with 3D printed bioceramic scaffolds *J. Dent. Res.* **97** 68–76
[56] Fischer E W, Sterzel H J and Wegner G 1973 Investigation of the structure of solution grown crystals of lactide copolymers by means of chemical reactions *Kolloid-Zeitschrift und Zeitschrift für Polym.* **251** 980–90
[57] Chen C *et al* 2003 Preparation and characterization of biodegradable PLA polymeric blends. *Biomaterials* **24** 1167–73
[58] Gill P, Moghadam T T and Ranjbar B 2010 Differential scanning calorimetry techniques: applications in biology and nanoscience *J. Biomol. Tech.* **21** 167–93 (https://www-ncbi-nlm-nih-gov.sheffield.idm.oclc.org/pmc/articles/PMC2977967/)
[59] Garlotta D 2002 A Literature Review of Poly (Lactic Acid). *Journal of Polymers and the Environment* **9** 63–8
[60] Kong Y and Hay J N 2003 The enthalpy of fusion and degree of crystallinity of polymers as measured by DSC *Eur. Polym. J.* **39** 1721–7
[61] Malina D, Biernat K and Sobczak-Kupiec A 2013 Studies on sintering process of synthetic hydroxyapatite *Acta Biochim. Pol.* **60** 851–855
[62] Lyu S and Untereker D 2009 Degradability of polymers for implantable biomedical devices *Int. J. Mol. Sci.* **10** 4033–65
[63] Azevedo H S and Reis R 2004 Understanding the enzymatic degradation of biodegradable polymers and strategies to control their degradation rate *Biodegradable Systems in Tissue Engineering and Regenerative Medicine* 1st (Boca Raton: CRC Press) 177–202
[64] De J W H *et al* 2005 Tissue response to partially in vitro predegraded poly- L -lactide implants. *Biomaterials* **26** 1781–91
[65] Almoatazbellah Youssef, Hollister Scott J and Dalton Paul D 2017 Additive manufacturing of polymer melts for implantable medical devices and scaffolds *Biofabrication* **9** 012002
[66] Anoopkumar-Dukie S *et al* 2005 Resazurin assay of radiation response in cultured cells *Br. J. Radiol.* **78** 945–7
[67] Hoque M E, Chuan Y L, Enamul Hoque P I M, Chuan Y L and Pashby I 2011 Extrusion based rapid prototyping technique: An advanced platform for tissue engineering scaffold fabrication *Biopolymers* **97** 83–93
[68] Laitinen O *et al* 1992 Mechanical properties of biodegradable ligament augmentation device of poly(l-lactide) *in vitro* and *in vivo Biomaterials* **13** 1012–6
[69] Bonuccelli G *et al* 2014 Role of mesenchymal stem cells in osteosarcoma and metabolic reprogramming of tumor cells *Oncotarget.* **5** 7575–88
[70] Mallick S, Tripathi S and Srivastava P 2015 Advancement in scaffolds for bone tissue engineering: a review *IOSR J. Pharm. Biol. Sci. Ver.* **10** 2319–7676
[71] Pereira Á and Oliva P 2014 Eficacia de la hidroxiapatita en la cicatrización de injertos óseos e implantes dentales: una revisión sistemática de la literatura hydroxyapatite effectiveness in healing of bone grafts and dental implants: a systematic review of the literature *Int. J. Odontostomat.* **8** 425–32
[72] Woodruff M A *et al* 2012 Bone tissue engineering: From bench to bedside *Mater. Today* **15** 430–5
[73] Cunniffe G M *et al* 2010 The synthesis and characterization of nanophase hydroxyapatite using a novel dispersant-aided precipitation method *J. Biomed. Mater. Res. - Part A.* **95** 1142–9
[74] Puwanun S 2014 *Developing a tissue engineering strategy for cleft palate repair.* University of Sheffield
[75] Heidari F *et al* 2017 Investigation of mechanical properties of natural hydroxyapatite samples prepared by cold isostatic pressing method *J. Alloys Compd.* **693** 1150–6
[76] Weir N A *et al* 2004 Degradation of poly-L-lactide. Part 2: increased temperature accelerated degradation *Proc. Inst. Mech. Eng. Part H J. Eng. Med* **218** 321–30
[77] Weir N A *et al* 2004 Degradation of poly-L-lactide *Part 1: in vitro and in vivo physiological temperature degradation.* **218** 307–19
[78] Felfel R M *et al* 2015 Accelerated *in vitro* degradation properties of polylactic acid/phosphate glass fibre composites *J. Mater. Sci.* 3942–55
[79] Garlotta D 2002 A literature review of poly (Lactic Acid) *J. Polym. Environ. [Internet].* **9** 63–84
[80] Felfel R M *et al* 2015 Accelerated *in vitro* degradation properties of polylactic acid/phosphate glass fibre composites *J. Mater. Sci.* **50** 3942–55
[81] Valente T A M *et al* 2016 Effect of sterilization methods on electrospun poly(lactic acid) (PLA) fiber alignment for biomedical applications *ACS Appl. Mater. Interfaces* **8** 3241–9
[82] Weir N A A *et al* 2004 Processing, annealing and sterilisation of poly-L-lactide *Biomaterials* **25** 3939–49
[83] Farrar D F and Gillson R K 2002 Hydrolytic degradation of polyglyconate B: the relationship between degradation time, strength and molecular weight *Biomaterials* **23** 3905–12
[84] Goosen M F A 1994 Investigation of poly (lactic acid) degradation please *J. Bioact. Compat. Polym.* **9** 80–100
[85] Cam D, Hyon S H and Ikada Y 1995 Degradation of high molecular weight poly(L-lactide) in alkaline medium *Biomaterials* **16** 833–43
[86] Li J *et al* 2009 Thermal degradation kinetics of g -HA/PLA composite. *Thermochimica Acta* **493** 90–5
[87] Lyu S P *et al* 2007 Kinetics and time-temperature equivalence of polymer degradation *Biomacromolecules.* **8** 2301–10
[88] Bose S *et al* 2010 Microwave-processed nanocrystalline hydroxyapatite: simultaneous enhancement of mechanical and biological properties *Acta Biomater.* **6** 3782–90
[89] Törmälä P 1992 Biodegradable self-reinforced composite materials; manufacturing structure and mechanical properties *Clin. Mater.* **10** 29–34